Journal of Structural Geology 33 (2011) 145–153

Contents lists available at ScienceDirect

Journal of Structural Geology

journal homepage: www.elsevier.com/locate/jsg

Strain pattern within and around denser blocks sinking within Newtonian salt structures

Steffi Burchardt [a,*], Hemin Koyi [a], Harro Schmeling [b]

[a] Department of Earth Sciences, University of Uppsala, Villavägen 16, 75236 Uppsala, Sweden
[b] Faculty of Earth Sciences, J. W. Goethe University, Altenhöferallee 1, 06438 Frankfurt am Main, Germany

ARTICLE INFO

Article history:
Received 16 June 2010
Received in revised form
5 November 2010
Accepted 17 November 2010
Available online 27 November 2010

Keywords:
Salt
Anhydrite
Deformation
Rheology
Gorleben

ABSTRACT

Blocks of dense material, such as anhydrite, entrained in salt structures have been proposed to sink through their host material. Here, we present the results of numerical models that analyse strain patterns within and around initially horizontal anhydrite blocks (viscosity 10^{21} Pa s) sinking through Newtonian salt with a viscosity of 10^{17} Pa s. In addition, the influence of the block aspect ratio (thickness to width ratio; AR) is analysed. The model results show that the blocks are folded and marginally sheared to approach streamlined shapes. The effectiveness of this process is a function of the block AR and influences the sinking velocity of the blocks significantly. Final sinking velocities are in the range of ca. 1.7 −3.1 mm/a. Around the block in the salt, an array of folds and shear zones develops during block descent, the structure of which is principally the same independent of the block AR. However, the size and development of the structures is a function of the block size. Monitoring of strain magnitudes demonstrates that the salt is subject to extremely high strains with successively changing stress regimes, resulting in closely-spaced zones of high adjacent to low strain. In comparison to the anhydrite blocks, strain magnitudes in the salt are up to one order of magnitude higher.

1. Introduction

Dense inclusions surrounded by a less viscous matrix occur in a variety of geological settings on practically all scales. Examples include anhydrite and limestone layers in salt structures (e.g. Bornemann, 1991), stoped blocks in magma chambers (Clarke et al., 1998), phenocrysts in magma (Arbaret et al., 2000), and englacial-morain material in glaciers (Talbot and Pohjola, 2009).The contrast in mechanical properties, such as density and viscosity, of these inclusions and their matrix has a strong influence on the strain pattern within the inclusion and the matrix.

Dense inclusions of synsedimentary anhydrite and limestone, as well as of extrusive and intrusive igneous rocks in salt structures are known from many locations worldwide, e.g. the salt diapirs in the North Sea and the North German Basin (Bornemann, 1991; Schleder et al., 2008), the Zagros Mountains, Iran (Kent, 1979; Gansser, 1992; Weinberg, 1993), Oman (Peters et al., 2003; Reuning et al., 2009), and Yemen (Davison et al., 1996a, b). These dense inclusions (or "stringers") have in most cases been entrained into salt diapirs during salt ascent (e.g. Jackson et al., 1990; Chemia et al., 2008). Consequently, they have been subjected to deformation as a result of the complex strain fields inside rising salt (Talbot and Jackson, 1987; Koyi, 2001). Recent investigations focus on the potential of some of these stringers as reservoirs for oil and gas (e.g. Al-Siyabi, 2005) as well as on their impact on the strain history of a salt structure. Following Weinberg's (1993) hypothesis that dense inclusions in salt may start to sink when the ascent rate of the salt is no longer sufficient to support their weight, Koyi (2001) and Chemia et al. (2009) demonstrated that sinking anhydrite slabs can reactivate the internal dynamics of a salt diapir, based on analogue and numerical modelling. This may have undesired effects on the long-term stability of disposal sites of hazardous waste, a number of which are planned in salt structures. Evidence that recent deformation around anhydrite blocks actually takes place comes from acoustic emissions recorded at the interface between anhydrite blocks and the surrounding rock salt in a German salt diapir (Spies and Eisenblätter, 2001). These acoustic signals may indicate the relative movement between the denser anhydrite blocks and their host salt diapir.

In this paper, we present results of numerical models that focus on the deformation produced by the sinking of a dense block through a less viscous matrix, particularly on the resulting structures within and around the block on block-scale. In order to get a basic understanding of the mechanical interaction of anhydrite blocks of different sizes and the surrounding salt, we analysed the strain associated with the gravity-driven descent of anhydrite blocks of different size through a body of salt representing a diapir.

* Corresponding author.
E-mail address: steffi.Burchardt@geo.uu.se (S. Burchardt).

0191-8141/$ – see front matter © 2010 Elsevier Ltd. All rights reserved.
doi:10.1016/j.jsg.2010.11.007

2. Model setup and methodological background

2.1. Scaling considerations and model setup

The models are not scaled to any particular case. However, the model setup and the material properties are based on natural examples. Dense inclusions in salt diapirs are in most cases of synsedimentary origin, including intraformational evaporites (e.g. anhydrite deposited as gypsum), carbonate layers and platforms, synsedimentary psammites, and even contemporaneous volcanic rocks (e.g. Gansser, 1992) with preserved sedimentary or igneous layering. Consequently, they are often characterised by tabular shapes (e.g. Gansser, 1960, 1992; Kent, 1979; Jackson et al., 1990), even though they have usually been deformed during salt ascent. The thickness and width of these inclusions is thus highly variable. A well-studied example of a salt diapir containing dense inclusions is the Gorleben salt diapir in Northern Germany that served as scaling constraint for our models. This diapir is 3 km wide and approximately 3 km thick in cross section (NW–SE). The original stratigraphic sequence building the diapir consists mainly of halite and potassium salt of Permian age (Zechstein, Staβfurt (z2) to Aller (z4) formations; Bornemann, 1991). The so-called Main Anhydrite (z3HA) is a sequence of anhydrite with minor carbonates and a thickness of up to 70 m. During ascent of the salt diapir the Main Anhydrite was entrained within the salt and subject to intense strain that resulted in folding, boudinage, and shearing. Consequently, the Main Anhydrite forms elongate boudins of approximately 100 to more than 1000 m length, partly folded into isoclinals folds together with the surrounding salt (Bornemann, 1991).

Each two-dimensional model consists of a 2000 m wide and 4000 m deep rectangular salt structure (Fig. 1). All sides of the model are defined as free-slip boundaries, i.e. displacement along the boundaries is enabled. Since all sides of the model represent symmetry planes and the model is lateral symmetric, only half of the model, i.e. a 1000 m wide and 4000 m deep rectangle, was modelled. At a depth of 100 m below the top of the model, a rectangular block with a higher density and viscosity, simulating a denser inclusion (e.g. anhydrite), is placed within the salt. The boundaries between the block and its matrix are adherent. The thickness of the block is 100 m, so that the block bottom is at an initial depth of 200 m. In order to understand the basic processes that control the mechanical interaction between blocks of denser material (anhydrite) and a viscous matrix (salt), we focus on one parameter: the size, and more specifically, the aspect ratio (AR; thickness to width ratio) of the anhydrite block. During ten successive model runs, the width of the block is varied from 100 m to 1000 m (thickness to width AR 1:1 to 1:10 respectively).

The salt is assigned a density of 2200 kg m^{-3}, while the density of anhydrite is defined as 2900 kg m^{-3}, considering a slightly lower density as compared to pure anhydrite (density 3000 kg m^{-3}), e.g. due to minor amounts of limestone. In each model, the block is allowed to sink within the salt structure driven by gravity alone due to the density contrast of 700 kg m^{-3}.

Experimental studies of rock salt subject to high strain rates show that salt rheology can vary from Newtonian to power-law behaviour depending on the interaction of various parameters, such as grain size, strain rate, brine content, the presence of impurities within the salt, and deviatoric stress (e.g. Urai et al., 1986, 2008; Van Keeken et al., 1993; Jackson et al., 1994). However, the rheological behaviour of salt at scales, temperatures, strain rates etc. relevant to natural systems is still not well understood and cannot be extrapolated from experimental results (cf. Urai et al., 1986). Estimations of salt rheology on diapir scale from natural examples conclude that salt may behave as a Newtonian fluid with viscosities in the range of 10^{15}–10^{21} Pa s (Mukherjee et al., 2010). In our models we therefore assigned the matrix material a linear viscosity of 10^{17} Pa s. We do not consider the influence of temperature, rheological contrasts or structural variations within the salt, i.e. the block sinks through an isotropic and homogeneous matrix of salt.

Despite a few studies on the rheology of anhydrite under experimental conditions (e.g. Müller and Siemes, 1974; Müller et al., 1981; Zulauf et al., 2009), little is known about the viscosity and deformation behaviour of anhydrite subject to natural strain rates and temperatures. Chemia et al. (2009) assumed a viscosity contrast between anhydrite and the surrounding salt of 10^{2}–10^{4}, while Zulauf et al. (2009) estimated it to be on the order of 10^{1} in their deformation experiments. We assigned the anhydrite block in our models a linear viscosity of 10^{20} Pa s, which gives rise to a viscosity contrast between the salt and the matrix of 10^{3}. This might be realistic considering that the anhydrite in natural salt diapirs, such as Gorleben, contains limestone with a higher viscosity.

Only the first 2000 m of sinking, where the block had reached a steady state, was used for analysis. When the block sinks beyond this depth, it starts to slow down as it "feels" the bottom boundary of the model. We therefore determined 2200 m as the final depth at which no boundary effects from the bottom can be expected.

2.2. Modelling strategy

The equations of conservation of mass, composition, and momentum defining the models were solved using a two-dimensional

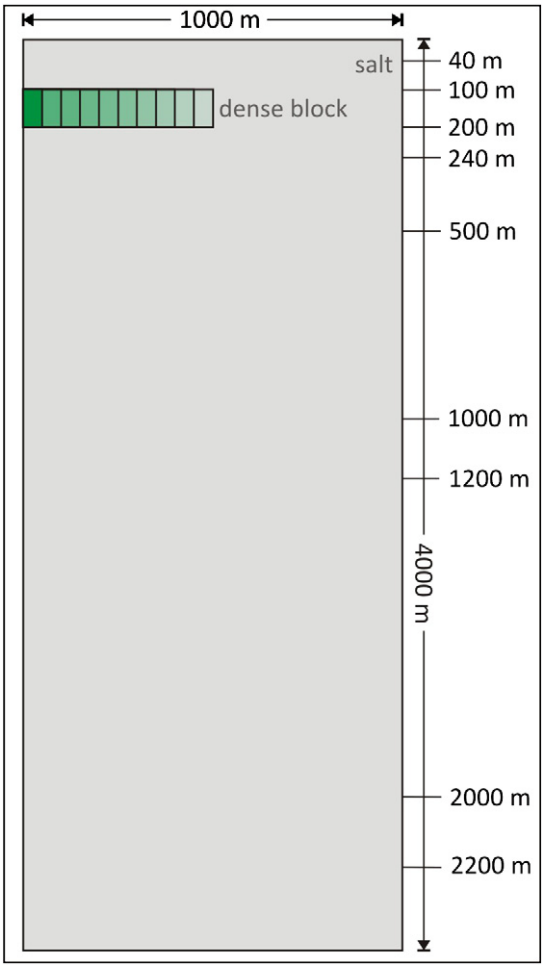

Fig. 1. Sketch of the model setup including the position of the block with higher density and viscosity (in green). (For interpretation of the references to colour in this figure legend, the reader is referred to the web version of this article).

finite differences code (FDCON; Weinberg and Schmeling, 1992) that uses a stream function formulation by applying Cholesky decomposition of the symmetric matrix. This code characterises the movement of compositional fields by a mesh of marker points that move according to a velocity field described by a fourth-order Runge–Kutta algorithm. In the current models, optimal results were ensured by a grid size of 101 times 401 with 1000 marker points in horizontal direction and 4000 marker points in vertical direction. Furthermore, in the models, materials are assumed to be incompressible, i.e., area changes do not occur, and characterised by a purely viscous, linear rheology so that elasticity is neglected. In addition, all inertial forces are neglected, i.e., creeping flow is assumed.

Interfaces between block and matrix material characterised by strong compositional contrasts (in this case defined by contrasts in density and viscosity) are resolved by defining effective parameters. This means that, e.g. the effective viscosity at each location along the interface is derived from the weighted sum of the viscosities of each material. For this purpose, the harmonic, arithmetic, or geometric mean of a parameter can be used (Schmeling et al., 2008). For our models, we used the arithmetic mean since it more accurately resolves the interface of the matrix with the more viscous block material. In comparison, the harmonic mean underestimates the density and viscosity of the outer parts of the block.

Strain pattern and magnitudes in and around the sinking block are described by the coordinates of the marker field. The strain field was calculated and plotted with the software SSPX (Cardozo and Allmendiger, 2009), using the grid nearest-neighbour method with a reduced data set of 100,000 grid points based on the equations by Ramsay (1967).

3. Results

3.1. Strain pattern and sinking velocity of the sinking block

The strain pattern within the anhydrite block is characterised by a sequence of marginal shear, internal folding, and minor marginal erosion. The exact succession, development, and intensity of each type of strain vary as a function of the block AR (Fig. 2). In the model with a square block (Fig. 2), the strain pattern within the block is characterised by marginal shear at the lateral boundaries, basal extension, and slight horizontal compression along the top boundary. In contrast, the block interior remains comparatively unstrained throughout the sinking process. During sinking, successive lateral shear results in the erosion of the lower block corners and an upward drag of block material along the sides of the block. The final shape of the block is characterised by rounded lower corners with a small amount of accumulated material dragged to the sides, forming appendices (Fig. 3). In comparison, a block with an AR of 1:5 (100 m thick and 500 m wide) is subject to marginal shear along the lateral boundaries that results in a slight rounding of the lower block corners (Fig. 2). At the same time viscous drag exerted by salt flow around the block causes horizontal extension of the lower block boundary and horizontal compression of the upper block boundary that leads to bending of the entire block during its sinking. During bending, the lateral block margins are continuously sheared. The final shape of the block, when it has descended 2000 m, is an open fold (interlimb angle 115°; Figs. 3 and 4). In comparison, a block with an AR of 1:10 is almost immediately folded after less than 100 m descent within the salt (Fig. 2). Marginal shear of the block occurs

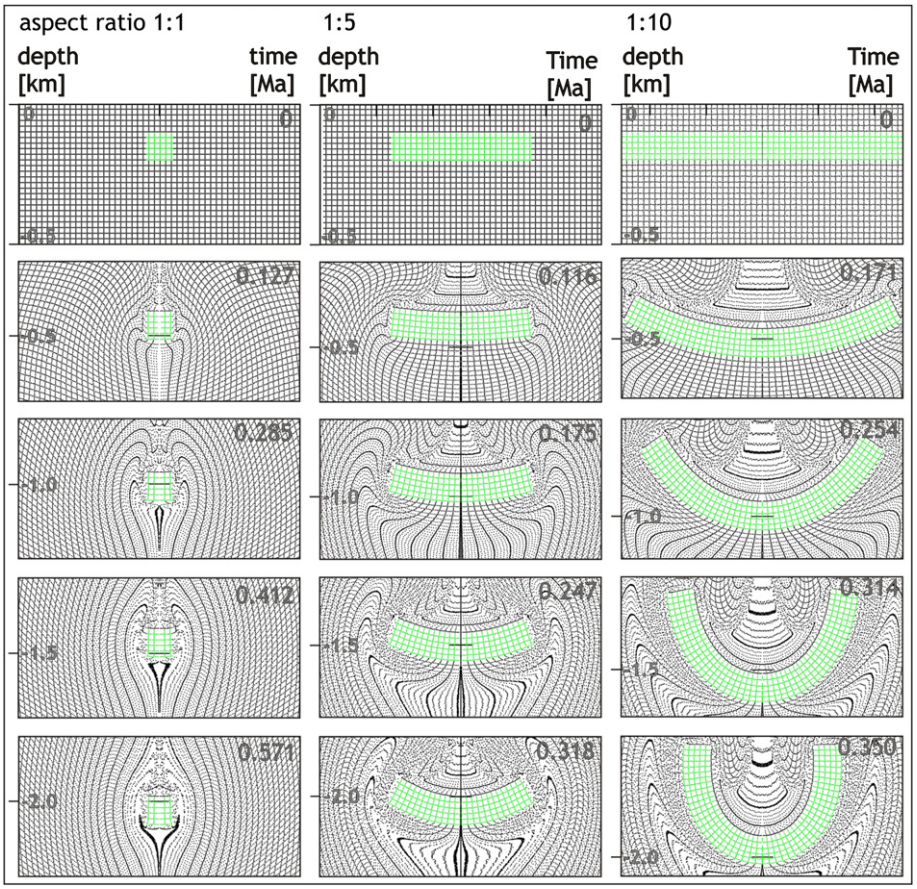

Fig. 2. Mesh plots of selected time steps during the sinking process of differently sized blocks (in green) surrounded by salt (in black). The mesh displays only every fifth row and line of the marker field. Each image shows a cut-out of 500 m depth and 1000 m width. The model has been flipped to show the full block geometry. (For interpretation of the references to colour in this figure legend, the reader is referred to the web version of this article).

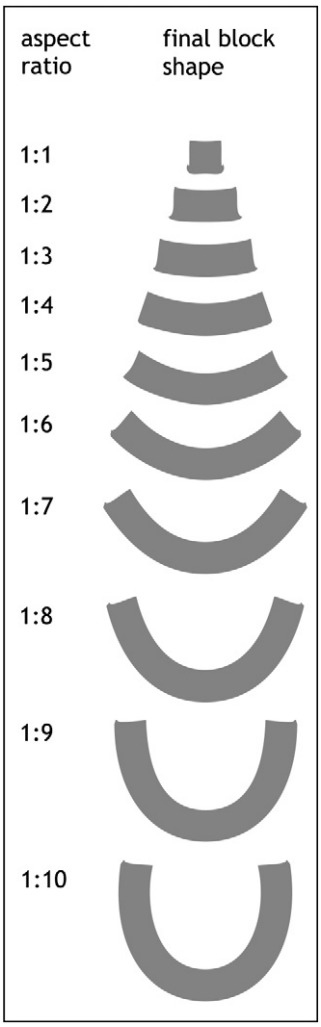

Fig. 3. Final block shape in the models with different block ARs after sinking below 2200 m.

only in the initial stages of sinking. Successive folding results in a horse-shoe shape with the limbs pointing towards each other, enclosing an angle of 10° at 2200 m depth (Fig. 4). Small appendices at the original lower block corners represent the effects of incipient lateral shear of the block sides.

The complete series of models shows that increasing the block AR results in a reduced intensity of marginal shear and erosion of the lower corners (Figs. 1 and 2). Instead, the block is subject to increasingly effective folding accompanied by increasing internal strain. For the viscosity contrasts used in the models, blocks with a low AR (1:1 to approximately 1:4) are less able to accommodate strain during sinking by folding. Hence, their horizontal orientation governs the strain pattern throughout their descent, which results in successive shear of the lateral block margins. In contrast, blocks with higher ARs (≥1:5) accommodate strain during sinking by folding and thus approach a streamlined shape (Fig. 3). This is also evident from the interlimb angle of the resultant folds that decreases continuously to result in isoclinals folds at block ARs of 1:9 and 1:10 (Fig. 4a). The same applies to the relative wave amplitude of the folds (Fig. 4b) that increases with block AR and the relative wave length (Fig. 4c) that decreases with increasing block AR.

The sinking velocity of the blocks was determined using the position of a single marker point in the block centre, 30 m above the lower block margin. The velocity profiles of the blocks (Fig. 5a) show that, at low ARs (1:1 to 1:4) after an initial acceleration phase the velocity only increases slightly to approach a constant velocity. The block with an AR of 1:1 has the lowest final velocity (1.68 mm/a), while the blocks with an AR of 1:4 and 1:5 reach the highest final velocities (3.05 and 3.07 mm/a; Fig. 5b). In contrast, at higher block ARs, an initial phase of low acceleration that probably coincides with the early phase of folding of the block is followed by a constant increase in velocity. The final velocities decrease with increasing block AR. The block with an AR of 1:10 reaches a final velocity of 2.80 mm/a. The velocity profiles are therefore not only a function of the increasing mass of the blocks. In order to test the effect of gravity on the sinking velocity, we ran a test model with a block of the same mass as the block with an AR of 1:10 but the same size and shape as the block with an AR of 1:1. The velocity profile of the block in this model is similar in shape to the profile of the block with an AR of 1:1, but with a much steeper slope (Fig. 5a) and an order of magnitude higher final velocity (64.41 mm/a). Hence, the aspect ratio, and thus the deformation path, of the block have a significant influence on its velocity pattern.

3.2. Strain pattern in the salt around the sinking block

The strain pattern within the salt during block descent shows that the salt below the block is vertically shortened and displaced sideways and upwards relative to the block (Fig. 6). The salt directly

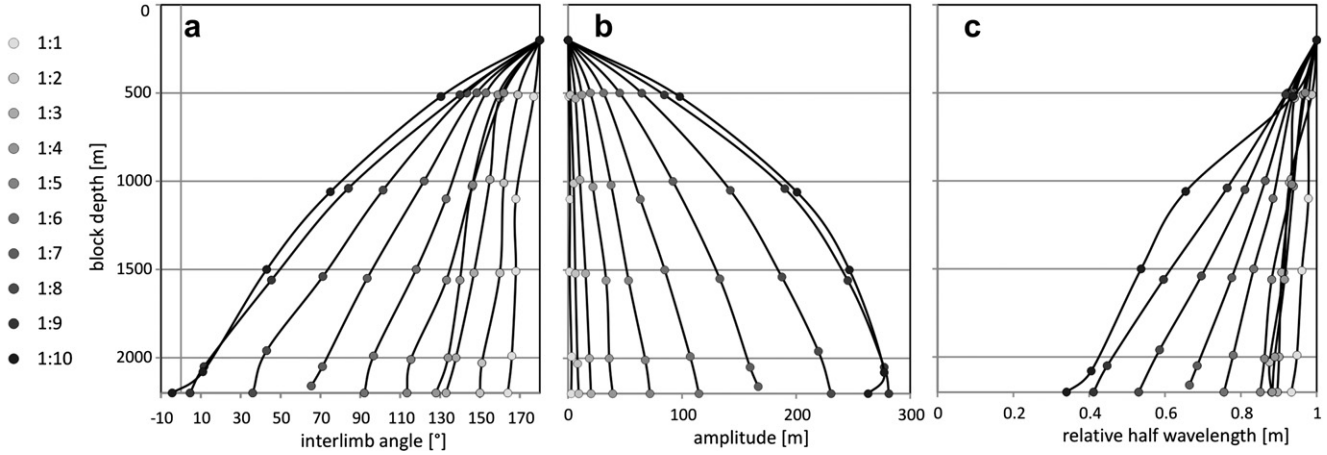

Fig. 4. Fold features of the blocks during sinking. The measurements were carried out using the upper block margins. a) Interlimb angle as a function of block width. b) Amplitude of the folds as a function of block width. c) Relative half-wave length (relative to the block width).

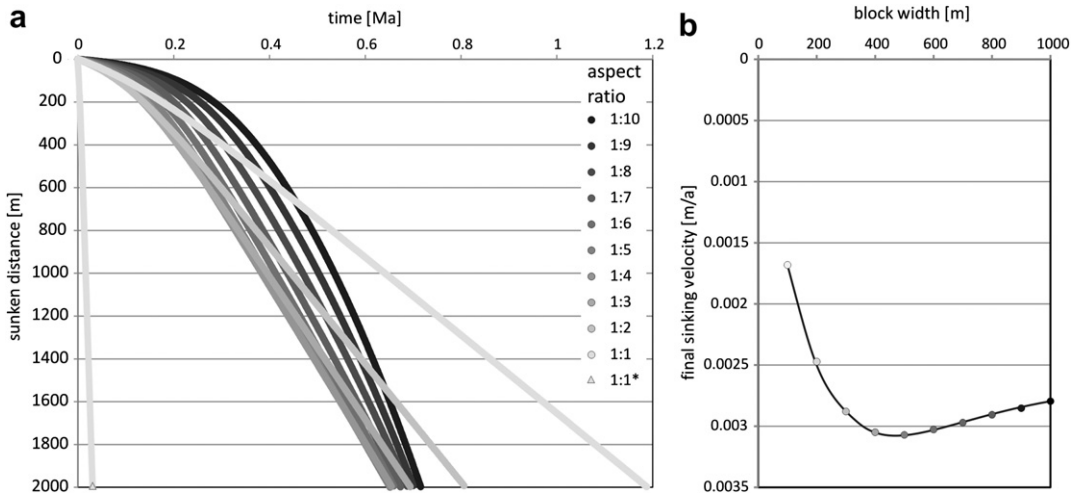

Fig. 5. a) Velocity profile of the blocks. The velocity profile of the model named 1:1* shows the sunken distance as a function of time of a block with an AR of 1:1 and the same mass as the block with an AR of 1:10. b) Final sinking velocity of the blocks as a function of block AR.

above the block is dragged downward together with the block within a narrow entrainment channel. This induces an inward and downward flow of the salt above the block. At the same time marginal synclines start to develop next to the block. In combination with the outward and upward flow of salt from below the block, this results in the formation of a marginal anticline adjacent to the syncline. During successive sinking, the downward movement of the block cannot be sufficiently compensated by folding of the salt. Consequently, zones of intense shear strain develop adjacent to the sides of the descending block. Additional shear zones form between the entrainment channel and the inward-flowing salt above the block caused by the much faster flow of material in the entrainment channel.

The structural characteristics of the strain pattern with folds and shear zones around the sinking blocks are the same for all blocks independent of their AR (Fig. 6). However, increasing the block AR causes the surrounding salt to be affected at a larger distance from the block. In addition, the entrainment channel above the block is considerably wider for blocks with a higher AR (Fig. 6). In the models with the higher block ARs (1:6 to 1:10), the area above the block between the entrainment channel and the marginal shear zone is characterised by an intense small-scale folding of the salt

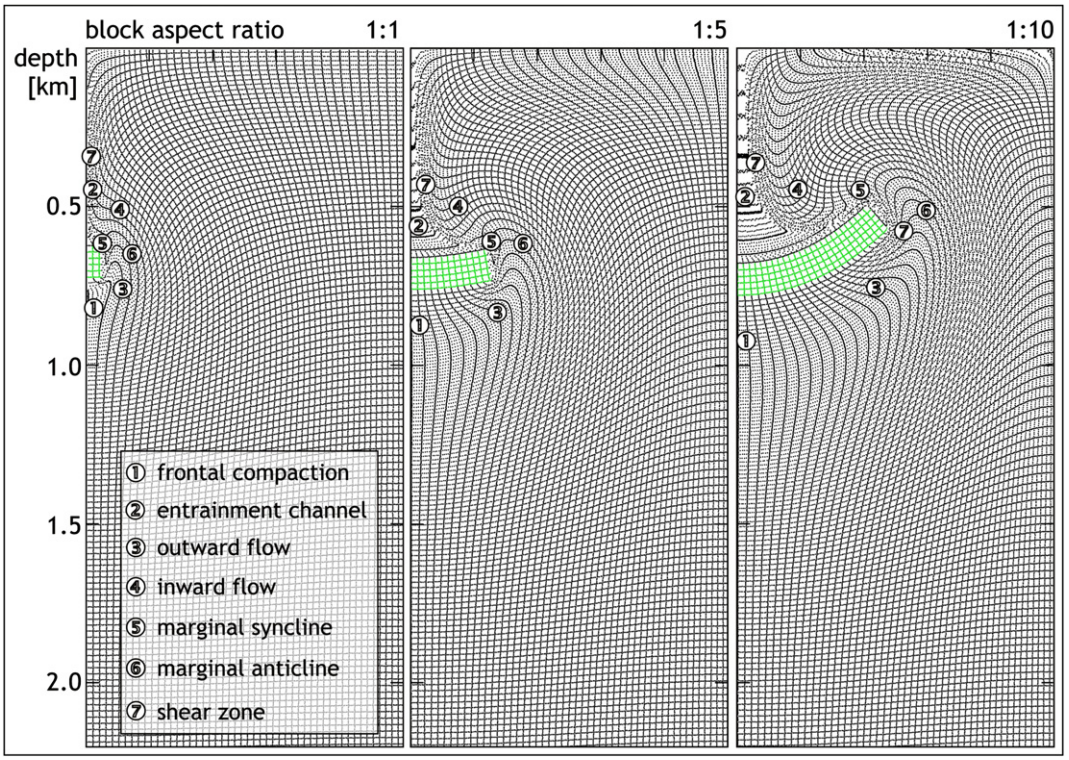

Fig. 6. Mesh plots of blocks (in green) with different AR surrounded by salt (in black) after ca. 500 m sinking. The mesh displays only every fifth row and line of the marker field. Each image is cut off at a depth of 2200 m. Numbers mark typical deformation features in the salt. (For interpretation of the references to colour in this figure legend, the reader is referred to the web version of this article).

that develops from the successive deformation and displacement of the earlier-formed marginal folds.

3.3. Strain magnitudes

A comparison of strain magnitudes and orientations within the sinking blocks shows that in general, the blocks are characterised by low strains that only increase slightly with increasing block AR (Figs. 7 and 8). Salt deformation during the sinking of the block is characterised by high strain (approximately one order of magnitude higher than in the block), concentrated mainly above the block in the entrainment channel and around the lateral ends of the block. In both locations, strong vertical elongation within the salt occurs (Fig. 8). Domains of high strain are not evenly distributed around the sinking block. Strain magnitude decreases rapidly away from the block in a pattern that mirrors the shear zones (highest strain magnitudes) and folds (high to intermediate strain magnitudes) described above (Fig. 6). Below the blocks with ARs >1, a strain shadow with a thickness of approximately 50–100% of the block thickness occurs. Below the strain shadow, the salt is vertically shortened and sheared (Figs. 7 and 8) as a result of salt flow from below the block to the sides (Fig. 6).

Extensional strain magnitudes in the salt depend on the block AR. Compared to the model with a block AR of 1:10, the maximum extensional strain in the model with a block AR of 1:1 is one order of magnitude lower (Fig. 7) while shear strain is approximately half (Fig. 8). While the distribution of high-strain zones in the salt is not a function of the block AR, the models show that the areal extent of strain around the block is strongly influenced by the block AR, i.e., that the area in the salt affected by the sinking block increases with increasing block AR.

4. Discussion

Our models show that the gravitational sinking of dense blocks or layer fragments of anhydrite through a Newtonian viscous medium (salt) causes severe deformation of the block and the matrix. This supports earlier experimental and numerical results by Koyi (2001) and Chemia et al. (2008, 2009) who modelled the entrainment and sinking of dense inclusions at diapiric scale using both Newtonian and power-law salt rheologies.

On block-scale, our models give a detailed account of the deformation history of the sinking block that is characterised by folding and shearing. According to Cruden (1990), the internal deformation of a gravity-driven viscous sphere is controlled by the viscosity contrast with the ambient material. Our models demonstrate that the internal deformation is also a function of the shape of the block. Initially horizontal blocks show more intense deformation at higher block ARs (Fig. 3). This has significant influence on the sinking velocity of the block, which is no longer a pure function of the block mass but strongly dependent on the ongoing deformation of the block that can considerably slow down the sinking rate (Fig. 5). Since our models are two-dimensional, the occurring strain is by definition plane strain. The three-dimensional nature of natural systems might result in different strain patterns though. In this respect, the calculations by Schmeling et al. (1988) demonstrate that around a rising (or falling) spherical body, the strain ellipsoid is oblate with the short axis pointing radially away from the rising body. In our models, equivalent results are observed (Fig. 8), except that the b-axis of the strain ellipsoid equals 1.

The salt surrounding the sinking block in our models accommodates high strain by the formation of a characteristic array of folds and shear zones, including a narrow channel of extreme

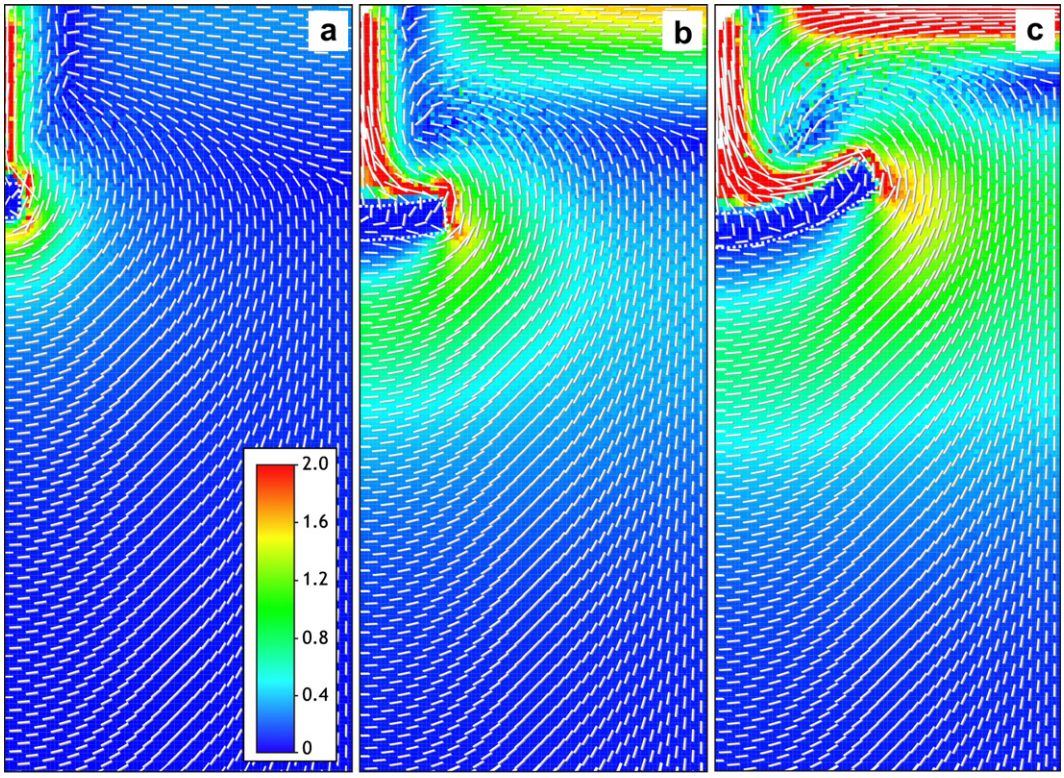

Fig. 7. Magnitudes (see coloured scale bar) and orientation (white ticks, only every 10th marker shown, scaled to 50% of their length) of extensional strain. Dashed line traces the block outline. Strain magnitudes were calculated with the grid nearest-neighbour method in SSPX (Cardozo and Allmendiger, 2009) with a grid spacing of 0.003, 9 nearest neighbours, and a maximum distance of grid points of 0.01, based on the coordinates of 100,000 marker points after 500 m of sinking of a block with an AR of a) 1:1, b) 1:5, and c) 1:10.

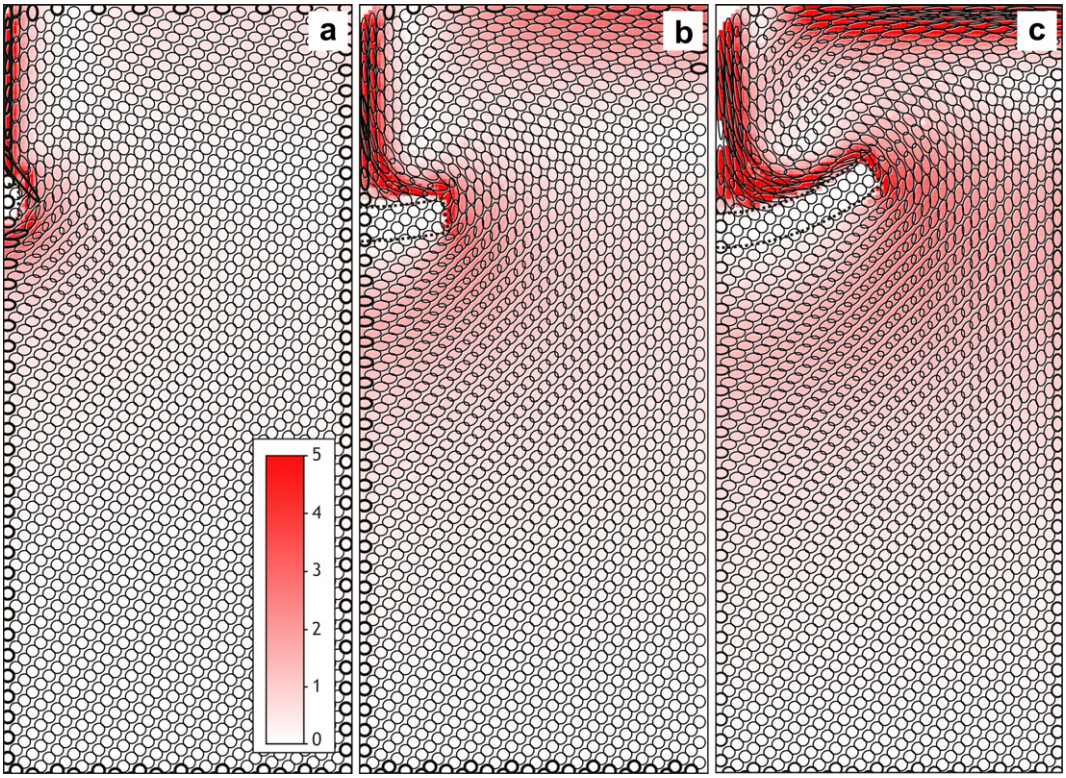

Fig. 8. Shear strain magnitudes (see coloured scale bar) and strain ellipses (only every 10th marker shown, size reduced to 25%) calculated with the grid nearest-neighbour method in SSPX (Cardozo and Allmendiger, 2009) with a grid spacing of 0.003, 9 nearest neighbours, and a maximum distance of grid points of 0.01, based on the coordinates of 100,000 marker points after 500 m of sinking of a block with an AR of a) 1:1, b) 1:5, and c) 1:10. Dashed line traces the block outline. (For interpretation of the references to colour in this figure legend, the reader is referred to the web version of this article).

stretching above the sinking block (Fig. 8). These structures are in accordance with numerical and experimental findings of Schmeling et al. (1988) and Cruden (1990) about the gravity-driven sinking of rigid and fluid spheres.

Natural systems are more complex and subject to a variety of parameters, the details of which cannot be accounted for in static numerical models. Apart from structural and compositional heterogeneities in the salt, complexities in natural systems may be caused by changes e.g. in the strain rate. Urai (pers. comm.; cf. Desbois et al., 2010) suggested that internal deformation in salt bodies may cease at low strain rates as a result of grain-boundary healing. Strain hardening associated with this process might be able to stabilise dense blocks within the salt. Evidence for this process might be the presence of anhydrite blocks in the highest levels of salt structures in the North Sea Basin that have been stable in this position for 60 Ma. Another unknown parameter as regards salt rheology and its response to the gravitational force exerted by denser blocks is the water content of both anhydrite and salt. Water in salt present as fluid inclusions or films along grain boundaries has a substantial effect on the rheological behaviour of the salt (Urai et al., 1986). On the other hand, water within the anhydrite and limestone might cause hydraulic fracturing of the anhydrite blocks causing them to behave much more brittle even at low strain rates (cf. Zulauf et al., 2009). In addition, water squeezed out of the anhydrite by deformation of the anhydrite might even fracture salt (Davison, 2009) or considerably weaken the interface between the block and the matrix so that the blocks might sink much faster (Leiss pers. comm.), a process that has been identified to be of major significance e.g. during shear deformation (Ildefonse and Mancktelow, 1993). Our model results therefore show strain patterns and magnitudes under relatively simplified homogeneous conditions. To model deformation associated with natural examples of anhydrite blocks in salt bodies, a more detailed understanding of the rheological input parameters is required.

Even though detailed studies of deformation structures around dense inclusions in salt structures are extremely scarce, structures analogue to those produced in our models occur around natural gravity-driven structures in a variety of other geological settings. The presented model results can be rescaled to other geological scenarios involving different dimensions, density contrasts, or viscosities. This can be achieved by multiplication of the length scale, velocity, and time by particular scaling factors. The strains will be the same for the same non-dimensional (relative) sinking distances, as long as the viscosity contrast is the same.

In general, diapiric structures, such as salt diapirs and plutons emplaced by diapirism are encased by high-strain aureoles characterised by the occurrence of ductile shear zones and/or brittle fault zones. Even though our models neglect temperature effects as those occurring around hot diapirs, similar highly strained zones also flank the blocks in our models. Furthermore, the rim synclines encircling natural diapirs correspond to the marginal anticlines that flank the sinking blocks in our models, while the tails of diapirs are equivalent to the entrainment channel (Fig. 6).

On a smaller scale, similar structures should be expected to occur in association with the development of a magmatic fabric in crystallising magmas. This system can, as a first approximation, be described as a dynamic suspension of rigid particles, the crystals, in an initially Newtonian matrix, the melt (Kerr and Lister, 1991; Arbaret et al., 2000). The settling or rise of the crystals in the melt generally follows Stokes equation (Stokes, 1851; Martin and Nokes, 1988), but also depends on the shape of the crystals (Kerr and Lister, 1991) and the fraction of crystals in the system (e.g. Arbaret et al., 2000). However, since the viscosity contrast between

melt and crystals is generally higher (in the range of several orders of magnitude) than in our models, strain within the settling crystals is much lower, while strain patterns produced by matrix flow around the settling crystals are in most cases not preserved.

In analogy, fragments of country rocks detached from the roof and walls of plutons by magmatic stoping should produce structures similar to those in the presented models. Stoped blocks sink through the magma driven by their higher density and may disturb a pluton's internal magmatic fabric, depending on the timing of sinking relative to the solidification of the pluton and the viscosity of the magma (Fowler and Paterson, 1997; Clarke et al., 1998). As regards the deformation of rock fragments entrained within magma, the effective viscosity of both, fragments and melt, as well as the viscosity contrast, has to be considered to draw conclusions from our model results. A viscosity contrast probably similar to the one in our models would explain deformation of autoliths in sheet-like magmatic intrusions (Correa-Gomes et al., 2001).

In addition, our model results show that strain magnitudes within the salt are in general much higher (in the range of one order of magnitude) than within the blocks. This indicates that strain is accommodated by the more viscous material. Within the salt, strain is not evenly distributed, neither does it decrease linearly away from the block. Instead, complex strain patterns are produced in the salt during the descent of the block.

These patterns consist of an array of folds and shear zones, the development and scale of which depend on the block AR. The determination of strain magnitudes demonstrates that the sinking of a block causes the formation of closely-spaced zones of low and high strains and that the salt around a sinking block experiences a complex strain history characterised by successively changing stress regimes. Sinking of dense blocks in nature should therefore be evident from the occurrence of similar structures in the vicinity of denser blocks, the observation of which might be limited by the outcrop conditions along the walls of salt mines.

5. Conclusions

Our models demonstrate that, using the defined material parameters, the gravitational force of a dense block exerted on the surrounding viscous matrix results in the block sinking through the matrix material. This process is accompanied by considerable strain, particularly around the block in the salt, that results in the formation of characteristic strain patterns. The block is sheared, folded, and marginally eroded to approach a streamlined shape. Around the block, an array of folds and shear zones develops in the salt, characterised by zones of high adjacent to low strains.

The main focus of our models was the influence of the thickness to width ratio (AR) of blocks within the range that occurs in natural salt bodies containing boudins of anhydrite. The model results demonstrate that the AR has considerable impact on the nature and magnitude of strain within and around the block, as well as on the sinking velocity of the block. A greater width of the block results in higher internal strain, evident from a more pronounced folding. The initial block AR and the efficiency of folding have a strong influence on the sinking velocity of the block that is even stronger than the effect of an increased mass with increasing block size (cf. Fig. 5). Final sinking velocities range of ca. 1.7–3.1 mm/a.

Strain is not homogeneously distributed throughout the salt; the highest strains occur above and along the lateral ends of the block. Our models show the development of characteristic structural domains around the sinking blocks, independent of their AR. These domains develop due to salt flow in response of the gravitational sinking of the block and include folds and shear zones in closely-spaced arrays with extreme contrasts in strain magnitudes. The block AR only accounts for the areal extent of these deformation zones in the salt, with larger areas affected by larger blocks (higher AR), and the development of these zones.

Acknowledgements

The authors are grateful to Zurab Chemia and Nestor Cardozo for help with data processing and to the members of the salt workshop at the TSK13 conference in Frankfurt for feedback and stimulating discussions. We also thank Stuart Hardy for suggesting to use SSPX for strain visualisation and him and Susan Treagus for thoughtful reviews. This project was funded by the Swedish Research Council (VR).

References

Al-Siyabi, H.A., 2005. Exploration history of the Ara intrasalt carbonate stringers in the South Oman salt basin. GeoArabia 10, 39–72.
Arbaret, L., Fernandez, A., Jezek, J., Ildefonse, B., Launeau, P., Diot, H., 2000. Analogue and numerical modelling of shape fabrics: application to strain and flow determination in magmas. Transactions of the Royal Society of Edinburgh: Earth Sciences 90, 97–109.
Bornemann, O., 1991. Zur Geologie des Salzstocks Gorleben nach Bohrergebnissen. Hannover, Germany. Bundesamt für Strahlenschutz Schriften, Saltgitter. 4, 67.
Cardozo, N., Allmendiger, R.W., 2009. SSPX: a program to compute strain from displacement/velocity data. Computers & Geosciences 35, 1343–1357.
Chemia, Koyi, H., Schmeling, H., 2008. Nomerical modelling of rise and fall of dense layers in salt diapirs. Geophysical Journal International 172, 798–816.
Chemia, Z., Schmeling, H., Koyi, H., 2009. The effect of the salt viscosity on future evolution of the Gorleben salt diapir, Germany. Tectonophysics 473, 446–456.
Clarke, D.B., Henry, A.S., White, M.A., 1998. Exploding xenoliths and the absence of 'elephants' graveyards' in granite batholiths. Journal of Structural Geology 20, 1325–1343.
Correa-Gomes, L.C., Souza Filho, C.R., Martins, C.J.F.N., Oliveira, E.P., 2001. Development of symmetrical and asymmetrical fabrics in sheet-like igneous bodies: the role of magma flow and wall-rock displacements in theoretical and natural examples. Journal of Structural Geology 23, 1415–1428.
Cruden, A.R., 1990. Flow and fabric development during the diapiric rise of magma. The Journal of Geology 98, 681–698.
Davison, I., 2009. Faulting and Fluid Flow through Salt. Journal of the Geological Society, London. 166, 1–12.
Davison, I., Alsop, I., Blundell, D., 1996a. Salt Tectonics: Some Aspects of Deformation Mechanics. Geological Society, London. Special Publications 100, 1–10.
Davison, I., Bosence, D., Alsop, G.I., Al-Aawah, M.H., 1996b. Deformation and Sedimentation Around Active Miocene Salt Diapirs on the Tihama Plain, Northwest Yemen. Geological Society, London. Special Publications 100, 23–39.
Desbois, G., Závada, P., Schléder, Z., Urai, J., 2010. Deformation and recrystallisation mechanisms in actively extruding salt fountain: microstructural evidence for a switch in deformation mechanisms with increased availability of meteoric water and decreased grain size (Qum Kuh, central Iran). Journal of Structural Geology 32, 580–594.
Fowler, T.K., Paterson, S.R., 1997. Timing and nature of magmatic fabrics from structural relations around stoped blocks. Journal of Structural Geology 19, 209–224.
Gansser, A., 1960. Über Schlammvulkane und Salzdome. Vierteljahrsschrift der Naturforschergesellschaft Zürich. 105, 1–46.
Gansser, A., 1992. The enigma of the Persian salt-dome inclusions. Eclogae Geologicae Helvetiae 85, 825–846.
Ildefonse, B., Mancktelow, N.S., 1993. Deformation around rigid particles: the influence of slip at the particle/matrix interface. Tectonophysics 221, 345–359.
Jackson, M.P.A., Cornelius, R.R., Craig, C.H., Gansser, A., Stocklin, J., Talbot, C.J., 1990. Salt diapirs of the Great Kavir, central Iran. Geological Society of America Memoirs 177 139pp.
Jackson, M.P.A., Vendeville, B.C., Schultz-Ela, D.D., 1994. Structural dynamics of salt systems. Annual Review of Earth and Planetary Sciences 22, 93–117.
Kent, P.E., 1979. The emergent Hormuz salt plugs of southern Iran. Journal of Petrological Geology 2, 117–144.
Kerr, R.C., Lister, J.R., 1991. The effects of shape on crystal settling and on the rheology of magmas. The Journal of Geology 99, 457–467.
Koyi, H., 2001. Modeling the influence of sinking anhydrite blocks on salt diapirs targeted for hazardous waste disposal. Geology 29, 387–390.
Müller, P., Siemes, H., 1974. Festigkeit, Verformabarkeit und Gefügeregelung von Anhydrit – Experimentelle Stauchverformung unter Manteldrucken bis 5 kbar bei Temperaturen bis 300°C. Tectonophysics 23, 105–127.
Müller, W.H., Schmid, S.M., Briegel, U., 1981. Deformation experiments on anhydrite rocks of different grain sizes: rheology and microfabric. Tectonophysics 78, 527–543.
Martin, D., Nokes, R., 1988. Crystal settling in a vigourously convecting magma chamber. Nature 332, 534–536.
Mukherjee, S., Talbot, C.J., Koyi, H.A., 2010. Viscosity estimates of salt in the Hormuz and Namakdan salt diapirs, Persian Gulf. Geological Magazine 147, 497–507.

Peters, J.M., Filbrandt, J.B., Grotzinger, J.P., Newall, M.J., Shuster, M.W., Al-Siyabi, H.A., 2003. Surface-piercing salt domes of interior North Oman, and their significance for the Ara carbonate "stringer" hydrocarbon play. GeoArabia 8, 231–270.

Ramsay, J.G., 1967. Folding And Fracturing Of Rocks. McGraw-Hill Book Company, New York, p. 568.

Reuning, L., Schoenherr, J., Heimann, A., Urai, J.L., Littke, R., Kukla, P., 2009. Constraints on the diagenesis, stratigraphy and internal dynamics of the surface-piercing salt domes in the Ghaba salt basin (Oman): a comparison to the Ara formation in the South Oman salt basin. GeoArabia 14, 83–120.

Schleder, Z., Urai, J.L., Nollet, S., Hilgers, C., 2008. Solution-precipitation creep and fluid flow in halite: a case study of Zechstein (Z1) rocksalt from Neuhof salt mine (Germany). International Journal of Earth Sciences 97, 1045–1056.

Schmeling, H., Cruden, A.R., Marquart, G., 1988. Progressive deformation in and around a fluid sphere moving through a viscous medium: implications for diapiric ascent. Tectonophysics 149, 17–34.

Schmeling, H., Babeyko, A., Enns, A., Faccenna, C., Funiciello, F., Gerya, T., Golabek, G.J., Grigull, S., Kaus, B., Morra, G., Schmalholz, S.M., van Hunen, J., 2008. A benchmark comparison of spontaneous subduction models – towards a free surface. Physics of the Earth and Planetary Interiors 171, 198–223.

Spies, T., Eisenblätter, J., 2001. Acoustic emission investigation of microcrack generation at geological boundaries. Engineering Geology 61, 181–188.

Stokes, G.G., 1851. On the effect of the internal friction of fluids on the motions of pendulums. Transactions of the Cambrian Philosophical Society 9, 1.

Talbot, C.J., Jackson, M.P.A., 1987. Internal kinematic of salt diapirs. American Association of Petroleum Geologists Bulletin 71, 1068–1093.

Talbot, C.J., Pohjola, V., 2009. Subaerial salt extrusions in Iran as analogues of ice sheets, streams and glaciers. Earth-Science Reviews 97, 155–183.

Urai, J.L., Spiers, C.J., Zwart, H.J., Lister, G.S., 1986. Weakening of rock salt by water during long-term creep. Nature 324, 554–557.

Urai, J.L., Schléder, Z., Spiers, C.J., Kukla, P.A., 2008. Flow and Transport Properties of Salt Rocks. In: Littke, R., Bayer, U., Gajewski, D., Nelskamp, S. (Eds.), Dynamics of Complex Intracontinental Basins: The Central European Basin System. Springer-Verlag, Berlin Heidelberg, pp. 277–290.

Van Keeken, P.E., Spiers, C.J., van den Berg, A.P., Muyzert, E.J., 1993. The effective viscosity of rock salt: implementation of steady-state creep laws in numerical models of salt diapirism. Tectonophysics 225, 457–476.

Weinberg, R.F., 1993. The upward transport of inclusions in Newtonian and power-law salt diapirs. Tectonophysics 228, 141–150.

Weinberg, R.F., Schmeling, H., 1992. Polydiapirs: multiwavelength gravity structures. Journal of Structural Geology 14, 425–436.

Zulauf, G., Zulauf, J., Bornemann, O., Kihm, N., Peinl, M., Zanella, A., 2009. Experimental deformation of a single-layer anhydrite in halite matrix under bulk constriction. Part 1: geometric and kinematic aspects. Journal of Structural Geology 31, 460–474.